# TENSILE BUCKLING OF ADVANCED TURBOPROPS

C. C. Chamis and R. A. Aiello
National Aeronautics and Space Administration
Lewis Research Center
Cleveland, Ohio 44135



## Introduction

The use of thin, highly swept, and twisted propeller blades (turboprops) is important to the development of efficient and quiet advanced aircraft (Fig. 1). The high sweep angle (as high as 60° for the turboprop reported herein) produces a significant reduction in noise and is, therefore, a desirable design feature. However, blades of this type (thin, highly swept, twisted) exhibit a complex state of structural response under a centrifugal force field requiring special analysis techniques.[1] These techniques are required to establish the rotor speed regions of various instabilities including tensile buckling. The objective of this paper is to describe theoretical studies which were performed at Lewis to determine analytically the tensile buckling of advanced titanium turboprops in centrifugal force fields, as well as the effects of tensile buckling on other types of structural behavior, such as resonant frequencies and flutter. Another objective of the paper is to identify any advantages of using "high performance" composite turboprops in order to change the regions of instability. The theoretical studies were performed using an in-house program designed for composite blade analysis. The turboprop geometry and material used, tensile buckling mechanisms (physics), tensile buckling predictions and tensile buckling effects on frequencies are described in detail. Several other aspects of tensile buckling on structural response such as shear forces at the hump (Fig. 1b), geometric coupling and material coupling, higher tensile buckling modes, nodal line shifting and flutter are also described.

## Turboprop Description

The simulated turboprop blade (propeller) used in the analysis is shown in Fig. 1. It is about 10 inches long, has a tip chord of 2 in., and a maximum chord at the hump of about 3.5 in. Thickness varies from 1 in. at midchord at the root to 0.040 in. at midchord at the tip. The leading edge thickness varies from 0.180 in. at the root to 0.022 in. at the tip. The trailing edge thickness varies from 0.077 in. at the root to 0.016 in. at the tip. The turboprop has a twist of 33.2° and tip sweep angle of 60°. The turboprop finite element analysis model is shown in Fig. 2. This model consists of 423 grid points and 744 CTRIA2 elements. The number of unrestrained degrees of freedom is 2466. First, a turboprop made from titanium was analyzed. Second, the titanium was replaced with high performance composites to determine the advantages of composites on the tensile buckling and the other instabilities. The high-performance composite was assumed to be type AS graphite-fiber/epoxy matrix at about 60 percent fiber by volume. Stiff ±45° plies were assumed to be made with fibers having 75 million psi modulus in order to study the shear stiffening effects.

## Tensile Buckling - Mechanisms

Tensile buckling occurs in swept turboprops because a compression-stress region develops at the hump (Fig. 3) under a centrifugal force field. The magnitude of the compression force in this region grows as the rotor speed is increased. Simultaneously, the boundary of the compression region grows because of the progressive change in the spatial position of the turboprop. This progressive change in spatial position produces changes in the direction and magnitude of the relative centrifugal acceleration and consequently changes in the centrifugal field. This region grows from the leading edge towards the center and along the span as the rotor speed is increased. The compression-stress region growth shown in Fig. 3 is for a simulated 60° swept titanium turboprop as the rotor speed increases from 1500 to 9000 rpm and accounting for spatial position changes.[1] The compression-stress region growth is greater along the span towards the tip than it is toward the center of the airfoil or towards the root.

As the rotor speed is increased, the compression-stress region continues to grow to a critical size at which elastic instability (buckling) is incipient. This elastic instability is identified, herein, as tensile buckling because it is induced by a tensile centrifugal force field. The corresponding rotor speed is identified as the tensile buckling rotor speed.

Tensile buckling of swept turboprops is analogous to the buckling of plates subjected to in-plane bending (Ref. 2, for isotropic plates and Ref. 3, for anisotropic plates). This in-plane bending in the hump region is induced by the swept portion of the turboprop because this portion tends to straighten out as the centrifugal force increases. The twist and the helical stacking axis also contribute to in-plane bending. For a qualitative example, the elemental vector equations for relative force and moment induced by an element $(\xi, \eta, \zeta)$ outboard of the hump on an element $(x, y, z)$ at the hump are, respectively (Fig. 4a),

$$\vec{\Delta F} = \Delta m \Omega_z^2 \left[(\xi - x)\, i + (\eta - y)\, j\right] \tag{1}$$

$$\vec{\Delta M} = \Delta m \Omega_z^2 \left[(\xi - x)(\eta - y)\, k + (\zeta - z)(\xi - x)\, j - (\zeta - z)(\eta - y)\, i\right] \tag{2}$$

where $\Delta m$ is the elemental mass at $(\xi, \eta, \zeta)$, $r_z$ is the rotor speed and $(i, j, k)$ are unit vectors corresponding to $(x, y, z)$.

Three interesting points can be identified in equations (1) and (2). First, any element outboard of the hump will induce a radial and a tangential force at the hump element. Second, the outboard element will induce three moments at the hump element: an in-plane moment (k), an out of plane moment (j), and a twisting moment (i). These moments induce one in-plane normal force, one in-plane shear and one through-the-thickness shear as will be described later. Third, and not as obvious, any small perturbations about an equilibrium position can have stabilizing or destabilizing effects on point

(x, y, z) depending on the perturbed position of ($\xi$, $\eta$, $\zeta$) relative to that at (x, y, z). This last point will be discussed later in more detail.

The integrated force and moment of all elements outboard of (x, y, z) can be determined by integrating equations (1) and (2) as ($\xi$, $\eta$, $\zeta$) varies from (x, y, z) to the tip of the turboprop. This integration is complex and not amenable to closed-form integration. However, the force variation across the chord through (x, y, z) can readily be obtained using finite element analysis. The in-plane force variation results for a special case (titanium turboprop, 6000 rpm, chord section at 5.5 in radius) is shown in Fig. 4(b). As can be seen, the in-plane compression forces at the leading edge are substantial. Also, the in-plane force variation across the chord is nonlinear.

Equations (1) and (2) can be combined to qualitatively assess the in-plane force variation if it is assumed that the turboprop is a plate of uniform thickness and lies in the (x-y) plane (Fig. 4(a)). The resulting elemental equation is:

$$\Delta N = \frac{\Delta m \Omega_z^2}{C} (\xi - x) \left[ 1 - \frac{12y}{C^2} (\eta - y) \right] \qquad (3)$$

where N is the in-plane force per unit chord and C is the chord width at the hump through (x, y). The first term in the brackets is due to in-plane force while the second is due to in-plane bending. Equation (3) is analogous to those described in Refs. 2 and 3 as mentioned previously. Equation (3) shows that the compression field is a function of spatial position and not of the rotational speed when the rotational speed is applied only in the initial turboprop position.

## Tensile Buckling - Prediction

The tensile buckling of the swept turboprops was predicted using COBSTRAN (Composite Blade Structural Analysis). COBSTRAN consists of composite mechanics, a blade finite element generator and NASTRAN.[4] Turboprops made from isotropic materials are handled as special cases in COBSTRAN. Since NASTRAN is a part of COBSTRAN, tensile buckling was predicted by using the NASTRAN Rigid FORMAT 5. Rigid FORMAT 5 predicts buckling, in general, using the differential stiffness methods.[5] The loading conditions, boundary conditions and solution methods are user supplied information within COBSTRAN which merges them with the NASTRAN bulk data prior to calling NASTRAN.

The procedure used for determining the rotor speed which will induce tensile buckling in turboprops is as follows:

1. Run COBSTRAN with a selected rotor speed (1500 rpm was used for the first speed).
2. Examine eigenvalue. Two cases are possible:
   a. Negative eigenvalue indicating no tensile buckling is possible, under this selected mode.
   b. Positive eigenvalue indicating the tensile buckling mode selected is possible.
3. If the eigenvalue is negative, increase rotor speed and/or select a

different mode, and run COBSTRAN again. The different mode is selected by specifying different eigenvalue ranges.

4. If the eigenvalue is positive, determine the rotor speed ($\Omega_{zcr}$) inducing tensile buckling from:

$$\Omega_{zcr} = \sqrt{\lambda^2}\,\Omega_z \tag{4}$$

where $\Omega_z$ is the rotor speed used and $\lambda^2$ is the eigenvalue predicted by NASTRAN.

5. Check $\Omega_{zcr}$ with at least two additional values of progressively greater rotor speeds ($\Omega$) to ascertain that the tensile buckling mode is the lowest mode represented by a positive eigenvalue.

Rotor speeds ($\Omega_{zcr}$) inducing tensile buckling in the 60° swept titanium and composite turboprops are summarized in Table 1. In addition, an unswept composite turboprop and a swept turboprop with stiff ±45° plies are included. The unswept turboprop is included to show that it does not have a possible tensile buckling mode. The swept turboprop with the stiff ±45° plies is included to illustrate increased shear-stiffness effect on tensile buckling speeds. The stiff ±45° plies were assumed to be made from a composite with a graphite fiber having 75 million psi modulus. The fiber modulus used in the other composites was assumed to be 32 million psi. All composite properties needed are generated within COBSTRAN.

It can be seen in Table 1 that

1. The titanium turboprop has about 15 percent higher tensile buckling rotor speeds then the composite.
2. Increased shear stiffness has negligible effects on the tensile buckling speed of composite turboprops.

The increased tensile buckling speed for the titanium turboprop is attributed, in part, to combinations of higher chordwise and shear stiffness of the titanium compared to composite even though the density of the composite is less. However, on rotor-speed-to-density basis (same airfoil volume for both), the tensile buckling speed for the composite turboprop is 182,500 rpm/lb compared to 77,940 rpm/lb for the titanium. This value translates to a 134 percent advantage for the tensile buckling speed of the composite turboprop over the titanium. The conclusion from the above discussion is that composite turboprops have a substantial weight advantage over titanium for the same tensile buckling speed.

The graphical representations of the eigenvalues as a function of rotor speed are shown in Fig. 5 for the unswept turboprop, in Fig. 6 for the 60° swept titanium turboprop and in Fig. 7 for the 60° swept composite turboprop. It can be seen in Fig. 5 that the eigenvalues remain negative throughout the rotor speed range of the unswept turboprop. Positive and negative eigenvalues for both swept turboprops are shown in Figs. 6 and 7. The negative eigenvalues are shown in order to illustrate that their existence does not preclude positive eigenvalues and, therefore, possible tensile buckling. Also, the asymptotic nature of the eigenvalues as the rotor speed approaches zero, or

infinity, is illustrated in Figs. 5 to 7. The lowest tensile buckling modes for both turboprops are shown in Fig. 8. The modes are about the same for both turboprops. The modes are primarily tip modes and are highly coupled since the out-of-plane and the in-plane displacements have about the same magnitude. The above discussion leads to the conclusion that rotor speeds that induce tensile buckling in swept turboprops can be determined from the procedures described herein.

## Tensile Buckling Effects on Frequencies

Tensile buckling effects on vibration frequencies of swept turboprops are similar to those of a compressive load on the frequencies of a structural component. For example, the equation of the lowest frequency of a vibrating beam subjected to a compressive load is given by[6]

$$\omega = \frac{\alpha\pi^2}{\ell^2}\left(\frac{EI}{M}\right)^{1/2}\left[1 - \frac{N}{N_{cr}}\right]^{1/2} \tag{5}$$

where $\omega$ is the lowest frequency, $\alpha$ is a constant depending on the boundary conditions, $\ell$ is the length, EI is the bending stiffness, m is the mass per unit length, N is the compressive force and $N_{cr}$ is the buckling load. The important point to be noted in equation (5) is that the frequency decreases as $N/N_{cr}$ increases and is zero where N equals $N_{cr}$.

The reduction in the vibration frequencies of the swept turboprops is not as severe as indicated in Equation (5). The reason is that the in-plane force induced by the centrifugal force field is not uniform, but varies as shown in Fig. 4(b). The qualitative vector elemental equations, corresponding to Equations (1) and (2) perturbed about an equilibrium steady-state postion by displacement fields with $(U_\xi, V_\eta, W_\zeta)$ at $(\xi, \eta, \zeta)$ and with $(U_x, V_y, W_z)$ at $(x, y, z)$, Fig. 4(a), are given by:

$$\vec{\Delta F} = \Delta m \Omega_z^2 \left\{\left[\xi - x + u_f - u_x\right] i + \left[\eta - y + v_\eta - v_y\right] j\right\} \tag{6}$$

$$\begin{aligned}\vec{\Delta M} = \Delta m L_z^2 \Big\{ & \left[(z - x)(\eta - y) + (u_\xi - u_x)(\eta - y) + (u_\xi - u_x)(v_\eta - v_y)\right] k \\ & + \left[(\zeta - z)(\xi - x) + (w_\zeta - w_z)(\xi - x) + (w_\zeta - w_z)(u_\xi - u_x)\right] j \\ & - \left[(\zeta - z)(\eta - y) + (w_\zeta - w_z)(\eta - y) + (w_\zeta - w_z)(v_\eta - v_y)\right] i \Big\}\end{aligned} \tag{7}$$

It can be seen in both Equations (6) and (7) that the changes in both force and moment can be stabilizing or destabilizing depending on the signs of the respective displacements $u_\xi$ and $u_x$, etc. Note the nonlinear geometric effects of displacement products $(u_\xi - u_x)(v_\eta - v_y)$, etc., on the elemental moment. The significance of these geometric nonlinear

effects depends on the displacement magnitudes which can be substantial if the displacements are of opposite sign. For example, the buckling mode shapes (Fig. 8 buckling mode shapes are comparable to vibration mode shapes) show substantial displacements at the tip but relatively small displacements at the hump.The integrated effects of these perturbations outboard of element (x, y, z) can be determined using COBSTRAN once a perturbed vibration shape has been selected.

The effects of possible tensile buckling on the frequencies of swept turboprops were predicted using COBSTRAN. The procedure used is that available in NASTRAN through Rigid FORMAT 13. The differential stiffness with appropriate eigenvalue extraction routines are used to calculate vibration frequencies and mode shapes of structural components in centrifugal force fields (geometric stiffening). The procedure used in NASTRAN for calculating vibration frequencies is similar to that used for calculating buckling described previously. The frequencies predicted are summarized in Table 2 for the titanium turboprop and in Table 3 for the composite.

The effects of possible tensile buckling on the vibration frequencies are best illustrated on a frequency versus rotor speed (Campbell) diagram. Results for the 60° swept composite turboprop are shown in Fig. 9. The frequencies (except the second) decrease as the tensile buckling rotor speed is approached. The first frequency is decreasing very rapidly and will be zero at the tensile buckling rotor speed. In contrast, the frequencies increase or remain about the same (second vibration mode, for example) with increasing rotor speed in the absence of compression force regions. One important observation in Fig. 9 is that no appreciable reduction in frequencies occurs prior to about 80 percent of the tensile buckling rotor speed.

The two important conclusions from the previous discussion are (1) the effects of tensile buckling on vibration frequencies in swept turboprops can be determined using available methods, and (2) tensile buckling has no appreciable reduction in the frequencies for rotor speeds less than 80 percent of the tensile buckling speed.

The interference of vibration frequencies with rotor excitation orders (such as one per revolution (1E), two per revolution (2E) etc.) are important in actual design practice. The influence of tensile buckling on frequency interference is shown in Fig. 10 for the swept composite turboprop assuming a 7500 rpm design rotor speed with ±10 percent margins. It is worth noting that the 5E engine excitation is the only one, and only slightly, within the operating margins of the fourth vibration mode frequency. It can also be seen that the margin between operating speed and tensile buckling is substantial.

It was mentioned previously that geometric nonlinearities may influence the vibration frequencies especially near the tensile buckling speed. Results reported in Ref. 1 show that the frequency of the fourth vibration mode of a 60° swept titanium turboprop was reduced significantly (about 30° percent) while the first three remained about the same. Methods described in Ref. 1 can be used to predict the geometric nonlinear effect when these are suspected to be substantial.

The previous discussion was only for turboprops with only 60° sweep angle. However, the collective steps of the method used constitute a struc-

tured procedure. This procedure can readily be used to study the effects of sweep angle on tensile buckling rotor speeds and the attendant structural responses.

## General Discussion

Several other structural aspects, in addition to the effects of tensile buckling on the structural response of swept turboprops, were studied during this investigation. These aspects are discussed here briefly because they are helpful in assessing the structural behavior of swept turboprops.

Shear Forces. In addition to the in-plane force at the hump (Fig. 4(b)) there are also two shear forces. One is in the plane and the other through the thickness. All of these forces are plotted versus percent chord in Fig. 11. The in-plane shear force ($F_z$) peaks near midchord with a magnitude comparable to the in-plane force ($F_x$). The through-the-thickness shear force ($F_y$) has the smallest magnitude. Its peak magnitude, near mid-chord, is about one-half of the in-plane shear force ($F_z$). All three forces contribute to tensile buckling. In addition, the through-the-thickness shear forces are important in assessing the interlaminar integrity of composite turboprops. For example, the maximum through-the-thickness shear stress at the hump in the composite turboprop at 7500 rpm will be about 570 psi, which is negligible, in this case, compared to that of the composite short-beam-shear strength of about 10 000 psi. The important observation to be noted is that swept, twisted composite turboprops have in-plane and through-the-thickness shear forces. These forces need to be considered in assessing the interlaminar integrity of composite turboprops in order to ascertain that the interlaminar shear stress is acceptable.

Geometric Coupling. The angle of sweep, the angle of twist and the stacking on the helix induce geometric coupling in the presence of a centrifugal force field. This coupling can be easily assessed by examining the stiffness matrix at a node, preferably at the tip. Stiffness matrices for the 60° swept titanium and composite turboprops are summarized in Table 4. These stiffness matrices were determined by applying successively a unit displacement in each direction at the tip mid-chord node while keeping the other five displacements fixed. The degree of geometric coupling is indicated by the off-diagonal terms which couple, for example, the radial displacement (u) to the other two forces ($F_y$ and $F_z$) and to the three moments ($M_x$, $M_y$, $M_z$). Note tnat the coupling of the three moments to the displacements (u, v, and w) is substantial. Note also the substantial coupling between the in-plane moment ($M_z$) and out-of-plane moment ($M_y$). These couplings are consistent with previous comments relative to equations (6) and (7). The presence of these couplings make it necessary to use finite element analysis to realistically evaluate the structural response of swept, twisted turboprops.

Material Coupling. Swept, twisted composite turboprops may also exhibit material coupling in addition to the geometric coupling just discussed. Material coupling in composites is present in either unsymmetric and/or unbalanced laminate configurations.[7] An indication of material coupling is obtained by normalizing the stiffness matrices in Table 4 and then by comparing corresponding coefficients. The normalized stiffness matrices are summarized in Table 5. Comparing corresponding coefficients, it is seen that (1) the

composite turboprop has greater in-plane coupling ($F_x$ with v and w, for example) than the titanium turboprop, and (2) both turboprops have about the same in-plane (membrane)/bending coupling ($F_x$ with $\theta_x$, $\theta_y$, and $\theta_z$, for example) and also about the same bending twisting coupling ($M_x$ with $\theta_y$ and $\theta_z$). The greater in-plane coupling ($F_x$ with w and u) is expected because of the greater Poisson's ratios of the (0±45) composite compared to titanium. Otherwise the turboprops are similar and differ only in density (0.16 lb/in$^3$ for titanium, 0.057 lb/in$^3$ for composite). The weights for the two simulated turboprops are: 0.70 lb for the titanium and 0.25 lb for the composite. One point worth noting is that the frequency improvements of the composite turboprop relative to the titanium (Table 2 and 3) are due mostly to the lighter density of the composite materials.

Higher Tensile Buckling Modes. It was mentioned previously that the tensile buckling speed should be ascertained with at least two values of progressively greater rotor speed. Frequently, the eigenvalue of higher modes is inadvertently calculated when the inverse power method is used as recommended in general purpose finite element programs. A plot of the buckling mode is the most direct way to ascertain which eigenvalue has been determined. For example, the second buckling mode for the composite turboprop is plotted in Fig. 12. This buckling mode is dramatically different from that for the first shown in Fig. 8. The rotor speed inducing tensile buckling at the second mode is about 22,000 rpm. This speed would readily be considered reasonable based on the square root of the density ratio and the tensile buckling speed of the titanium turboprop. Obviously 22,000 rpm is twice as great as the lowest speed (about 11,000 rpm) inducing tensile buckling in the composite turboprop. This example further illustrates the need to check the tensile buckling speed with progressively higher rotor speeds and with plots of the associated tensile buckling mode.

Vibration Mode Shapes. The vibration mode shapes are of interest because they show graphically the areas of predominant motion. The effects of rotor speed on the mode 1 vibration are shown in Fig. 13 for four different rotor speeds. The mode shapes shown are for maximum amplitude from the undeformed position. As can be seen, the motion is mostly at the tip. The motion appears to change from bending to bending/torsion coupling as the rotor speed is increased. The shapes of four different vibration modes are shown in Fig. 14 assuming an operating speed of 7500 rpm. These shapes indicate coupled motion.

Nodal Lines Shifting. The coupled motion is better illustrated by the effects of rotor speed on nodal line shifting as shown in Fig. 15 for the first vibration mode. The nodal line shifts slowly initially and then dramatically as the rotor speed is increased. The vibration mode up to 6000 rpm is predominately bending. However, it changes to torsional at 9000 rpm. It may be going through a "jumping" phenomenon at 7500 rpm, as shown by the single node point at the leading edge near the tip, prior to changing to the torsional mode. The nodal lines for the four different modes at 7500 rpm are shown in Fig. 16. These nodal lines indicate the coupled vibration motion of 60° swept turboprops. The coupled vibration motion is mostly at the tip and includes some chordwise modes. The coupled vibration modes and the progressive shifting of the nodal lines with increasing rotor speed make it highly questionable whether the dynamic response and flutter of swept turboprops can be assessed using beam modes or even finite element predicted modes at zero rotor speed.

Flutter. Determination of flutter requires complex aeroelastic calculations in general. However, an assessment can be obtained using the reduced velocity concept and assuming torsional flutter occurs first at operational speeds. Vibration mode three appears to be predominantly torsional in Fig. 16. The corresponding frequency for this vibration mode is 486.1 Hz (Table 2) for the titanium and 561.1 Hz (Table 2) for the composite. The various parameters and the equation required to calculate the reduced velocity are summarized in the appendix. Using these frequencies, the reduced velocity for the titanium turboprop is 2.09 and that for the composite is 1.81. Both of these values are substantially higher than the 1.5 value considered as an upper bound on torsional flutter. Both simulated turboprops will flutter near the assumed operational speed of 7500 rpm based on this assessment. It is interesting to note that the reduced velocity for the unswept turboprop is 0.83 which is well below 1.5. The important point from the above discussion is that torsional flutter depends on vibration mode shape and frequency. The effects of tensile buckling on flutter can be assessed through the selection of the mode shape and frequency used in calculating the reduced velocity. This example illustrates that flutter analysis for swept turboprops will generally require mode shapes and frequencies which are (1) coupled, (2) dependent on rotational speed, and (3) affected by tensile buckling.

## Summary

The significant results of an investigation on the tensile buckling of swept advanced propeller blades (turboprops) are as follows:

1. Rotor speeds that can induce tensile buckling of swept turboprops are readily determined from the procedure described herein.

2. Tensile buckling has negligible effects on vibration frequencies when the rotor speed is less than 80 percent of the tensile buckling speed.

3. Tensile buckling occurs in swept turboprops because the centrifugal force field induces substantial in plane compressive forces at the hump.

4. Composite turboprops have a substantial advantage (about 130 percent) over titanium on a tensile buckling speed to weight basis, However, the titanium turboprops have about 15 percent greater tensile buckling speed.

5. Increased shear stiffness has negligible effect on the tensile buckling speed of composite turboprops.

6. The buckled mode shapes are primarily tip modes and are extensively coupled.

7. The vibration mode shapes are coupled and exhibit substantial tip motion including some chordwise modes.

8. The vibration mode nodal lines shift with increasing rotor speed indicating dramatic changes in vibration mode shapes.

9. Substantial geometric coupling is present in both turboprops, but no material coupling exists even in the composite, other than that due to Poisson's effect.

10. The collective steps of the method used constitute a structured procedure to study the tensile buckling of swept turboprops and the attendant structural responses.

## References

1. Aiello, R. A. and Chamis, C. C., "Large Displacement and Stability Analysis of Nonlinear Structures," National Aeronautics and Space Administration, Washington, DC, NASA TM-82850, 1982.

2. Timoshenko, S. P. and Gere, J. M., Theory of Elastic Stability, 2nd ed., McGraw-Hill, New York, 1961, pp. 373-379.

3. Lekhnitskii, S. G., Anisotropic Plates, Gordon and Breach, New York, 1968, pp. 459-465.

4. Chamis, C. C., "Integrated Analysis for Engine Structures," NASA TM-82713, 1981.

5. McNeal, R. H., "The NASTRAN Theoretical Manual (Level 15.0)," NASA SP-221(01), 1972, Section 7.

6. Timoshenko, S., Young, D. H., and Weaver, W., Jr., Vibration Problems in Engineering, 4th ed., John Wiley and Sons, New York, 1974.

7. Chamis, C. C., "Computer Code for the Analysis of Multilayer Fiber Composites-User's Manual," NASA TN D-7013, 1971.

## Appendix

Summary of parameters used in the reduced velocity calculations in order to estimate possible torsional flutter.

### Assumed

| | |
|---|---|
| Mach number | 0.8 |
| Altitude | 35,000 ft |
| Engine speed | 7,500 rpm |
| 70 percent span radius | 0.75 ft |
| Air temperature at altitude | -60°F |
| Chord angle at 70 percent span | 12.9° |
| Half-chord at 70 percent span | 0.15 ft |

### Calculated

| | |
|---|---|
| Tangential velocity at 70 percent span ([(7500 x 2)/60] x 0.75) | 589.1 ft/sec |
| Speed of sound in air ($49.04\sqrt{400}$) | 980.8 ft/sec |
| Air speed (0.8 x 980.8) | 784.6 ft/sec |
| Relative air velocity ($(589.1^2 + 784.6^2)^{1/2}$) | 981.1 ft/sec |
| Angle of incidence ($\tan^{-1}$ (589.1/784.6) - 12.9°) | 13.0° |
| Velocity along chord (981.1 x cos 13°) | 956.0 ft/sec |

### Reduced Velocity Equation

$$V_r = \frac{Vc}{b\,\omega}$$

where

$V_r$ reduced velocity
$V_c$ air speed along chord, ft/sec
$b$ half-chord, ft
$\omega$ torsional frequency, rad/sec

TABLE 1

Summary of Tensile Buckling Speeds

| Turboprop | Rotor Speed (rpm) at Tensile Buckling |
|---|---|
| Unswept - Composite | N/A |
| Swept - Titanium | 12 470 |
| Swept - Composite | 10 950 |
| Swept - Composite (Stiff ±45 Plies) | 11 370 |

NOTE: N/A - Not Applicable (unswept turboprops are not subject to tensile buckling).

TABLE 2

Summary of Frequencies for Swept

Titanium Turboprop

| Rotor speed, rpm | Frequency, Hz, for vibration mode - 1 | 2 | 3 | 4 |
|---|---|---|---|---|
| 0 | 101.6 | 235.0 | 488.0 | 554.2 |
| 2500 | 117.1 | 241.7 | 487.7 | 571.2 |
| 5000 | 151.6 | 255.0 | 491.2 | 618.6 |
| 6500 | 174.1 | 261.6 | 488.7 | 655.8 |
| 7500 | 187.6 | 265.2 | 486.1 | 680.8 |
| 9000 | 200.0 | 270.5 | 475.0 | 711.2 |

NOTE: Frequencies predicted using COBSTRAN

TARLE 3

Summary of Frequencies for Swept

Composite Turboprop

| Rotor speed, rpm | Frequency, Hz, for vibration mode - 1 | 2 | 3 | 4 |
|---|---|---|---|---|
| 0 | 149.3 | 295.2 | 589.0 | 653.1 |
| 3000 | 161.8 | 295.5 | 585.7 | 678.4 |
| 4500 | 174.1 | 295.3 | 580.8 | 708.7 |
| 6000 | 185.2 | 294.7 | 572.8 | 748.6 |
| 7500 | 188.0 | 295.6 | 561.1 | 795.4 |
| 9000 | 169.4 | 301.4 | 544.6 | 843.5 |

NOTE: Frequencies predicted using COBSTRAN

TABLE 4

Stiffness Matrices at Tip Midchord
[60° Swept Turboprops]

(a) Titanium

$$\begin{Bmatrix} F_x \\ F_z \\ F_y \\ M_x \\ M_z \\ M_y \end{Bmatrix} = \begin{bmatrix} 4231 & 1735 & 1851 & 276 & -322 & -128 \\ & 1547 & 1124 & 310 & -185 & -25 \\ & & 1017 & 151 & -127 & -36 \\ & & & 240 & -107 & 5 \\ & \text{Symmetric} & & & 125 & 49 \\ & & & & & 34 \end{bmatrix} \begin{Bmatrix} u \\ w \\ v \\ \theta_x \\ \theta_z \\ \theta_y \end{Bmatrix}$$

(b) Composite

$$\begin{Bmatrix} F_x \\ F_z \\ F_y \\ M_x \\ M_z \\ M_y \end{Bmatrix} = \begin{bmatrix} 2342 & 1246 & 1151 & 215 & -191 & -59 \\ & 1136 & 844 & 203 & -122 & -17 \\ & & 712 & 110 & -80 & -18 \\ & & & 129 & -76 & -9 \\ & \text{Symmetric} & & & 74 & 25 \\ & & & & & 14 \end{bmatrix} \begin{Bmatrix} u \\ w \\ v \\ \theta_x \\ \theta_z \\ \theta_y \end{Bmatrix}$$

TABLE 5

Normalized Stiffness Matrices at Tip Midchord
[60° Swept Turboprops]

(a) Titanium

$$\begin{Bmatrix} F_x \\ F_z \\ F_y \\ M_x \\ M_z \\ M_y \end{Bmatrix} = \begin{bmatrix} 1.00 & 0.41 & 0.44 & 0.07 & -0.08 & -0.030 \\ & 0.37 & 0.27 & 0.07 & -0.[illegible] & -0.006 \\ & & 0.24 & 0.04 & -0.03 & -0.008 \\ & & & 0.06 & -0.03 & -0.001 \\ \text{Symmetric} & & & & 0.03 & 0.012 \\ & & & & & 0.008 \end{bmatrix} \begin{Bmatrix} u \\ w \\ v \\ \theta_x \\ \theta_z \\ \theta_y \end{Bmatrix}$$

(b) Composite

$$\begin{Bmatrix} F_x \\ F_z \\ F_y \\ M_x \\ M_z \\ M_y \end{Bmatrix} = \begin{bmatrix} 1.00 & 0.53 & 0.50 & 0.09 & -0.08 & -0.025 \\ & 0.49 & 0.36 & 0.07 & -0.05 & -0.007 \\ & & 0.30 & 0.05 & -0.03 & -0.008 \\ & & & 0.06 & -0.03 & 0.004 \\ \text{Symmetric} & & & & 0.03 & 0.011 \\ & & & & & 0.006 \end{bmatrix} \begin{Bmatrix} u \\ w \\ v \\ \theta_x \\ \theta_z \\ \theta_y \end{Bmatrix}$$

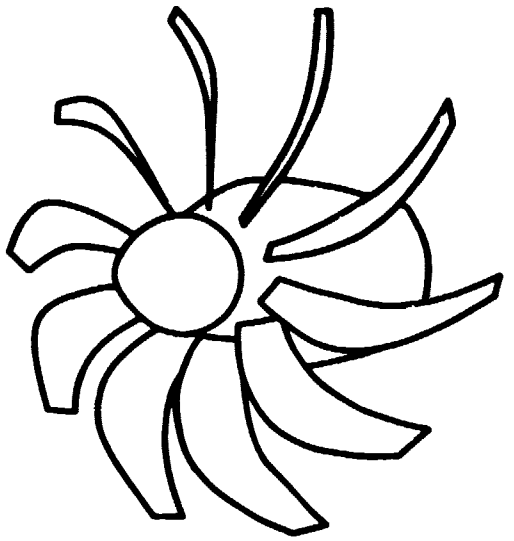

(a)

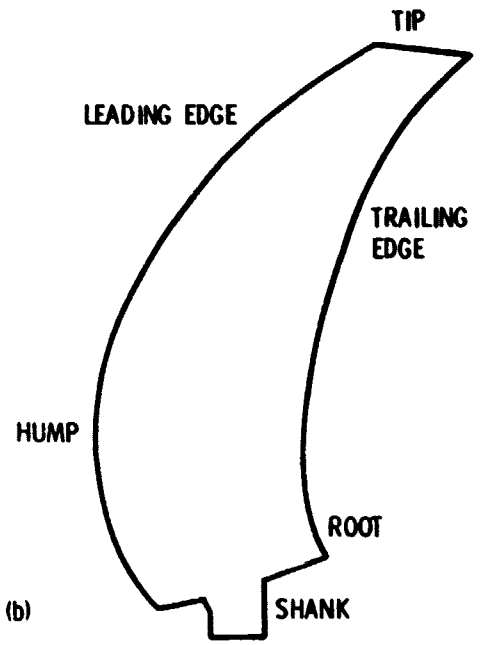


(b)

(a) Stage.
(b) Propeller blade (turboprop).

Figure 1. - Turboprop stage and propeller blade (turboprop).

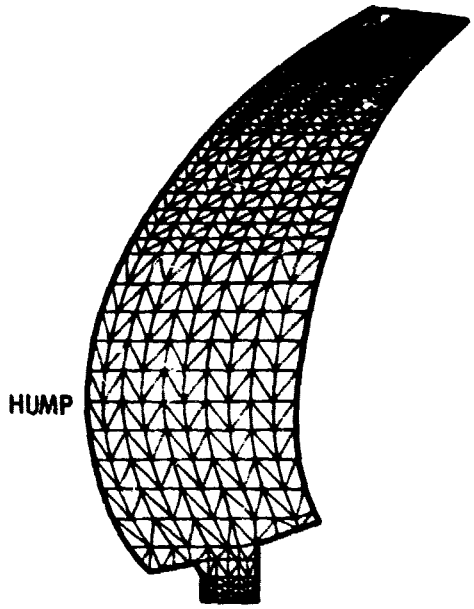


Figure 2. - Turboprop propeller finite element model (423 grid points, 744 elements).

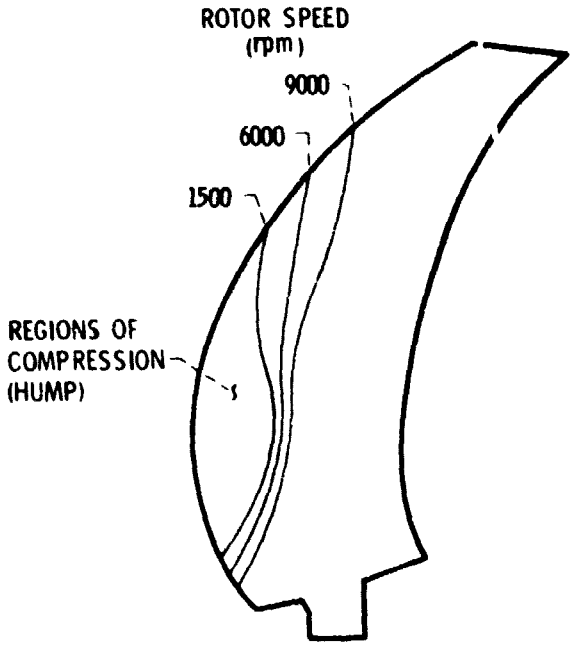


Figure 3. - Turboprop propeller compression regions from centrifugal force field.

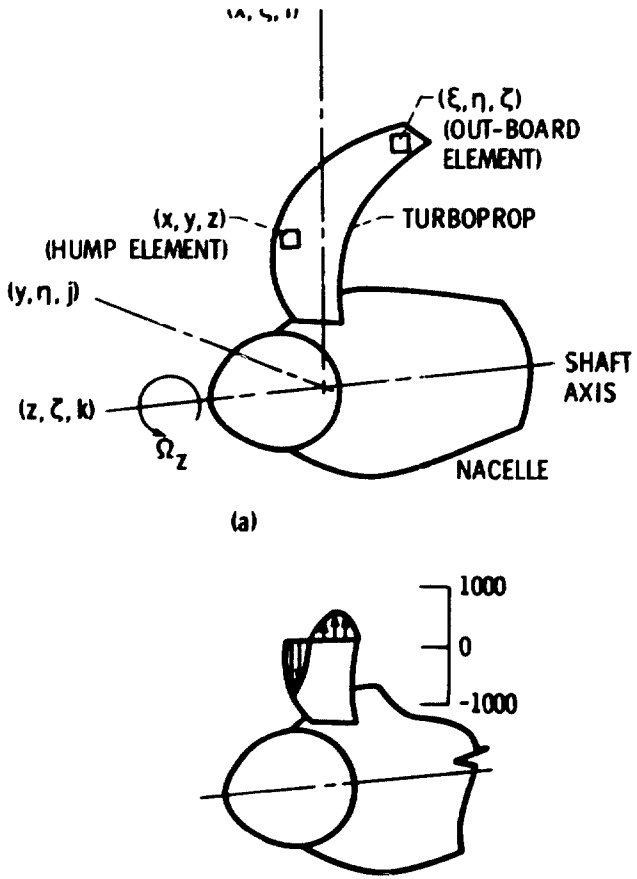


(a) Geometry

(b) In plane force
(x = 5.5 in.;
$\Omega_z$ = 6000 rpm)

Figure 4. - Schematic depicting source of compression forces in the hump region of swept turboprops.

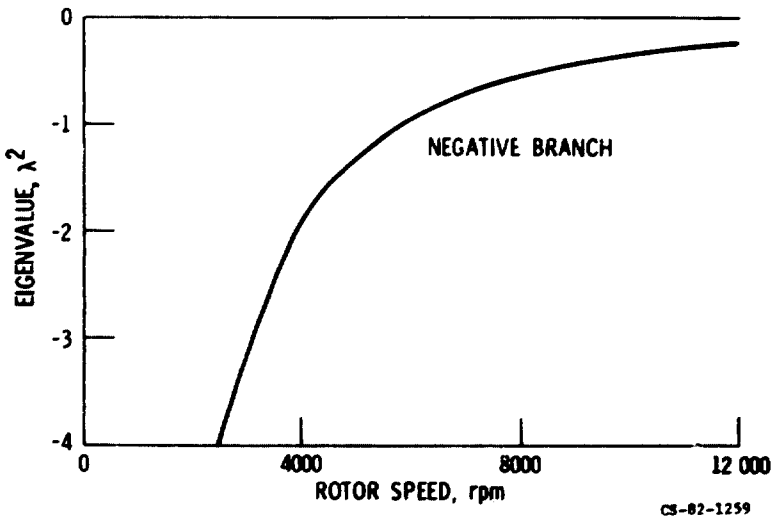


Figure 5. - Eigenvalues of unswept composite turboprops.

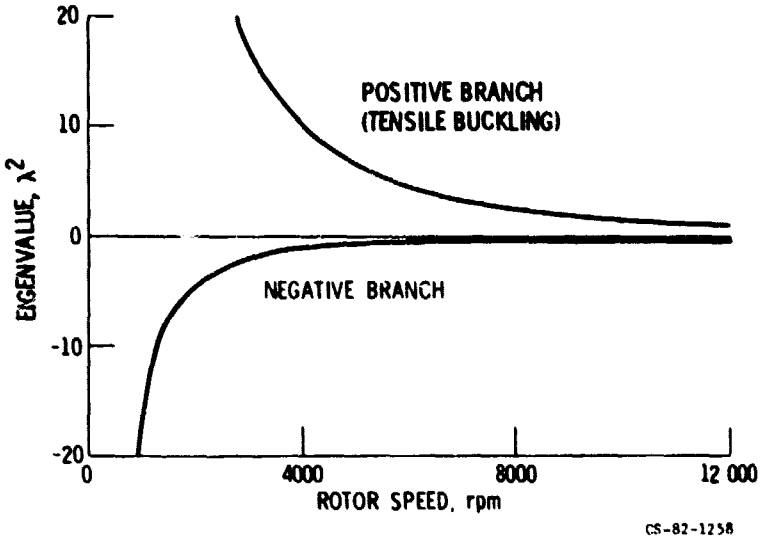


Figure 6. - Eigenvalues of $60^0$ swept titanium turboprop.

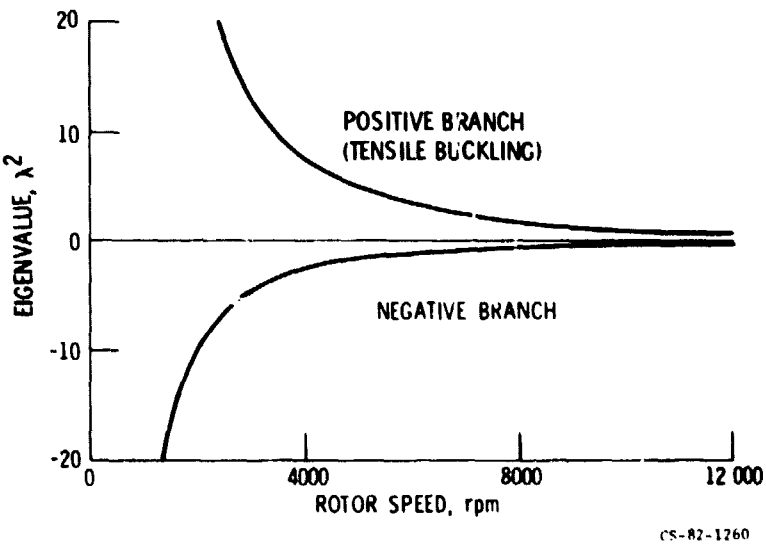


Figure 7. - Eigenvalues of $60^0$ swept composite turboprop.

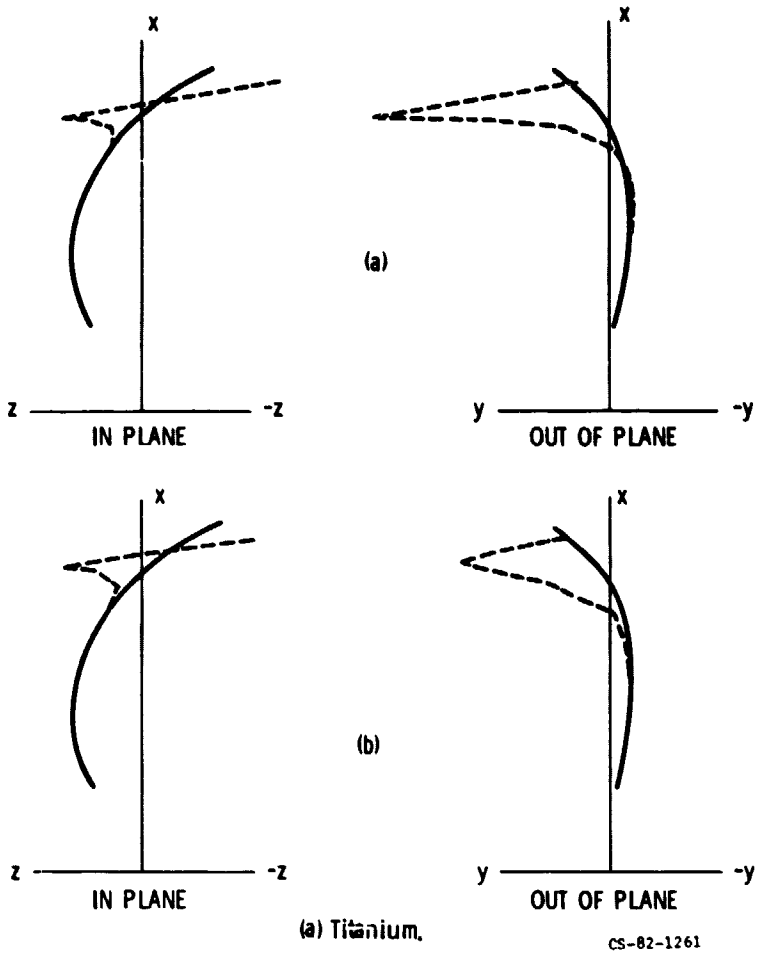


Figure 8. - Tensile buckling modes of 60° swept turboprops.

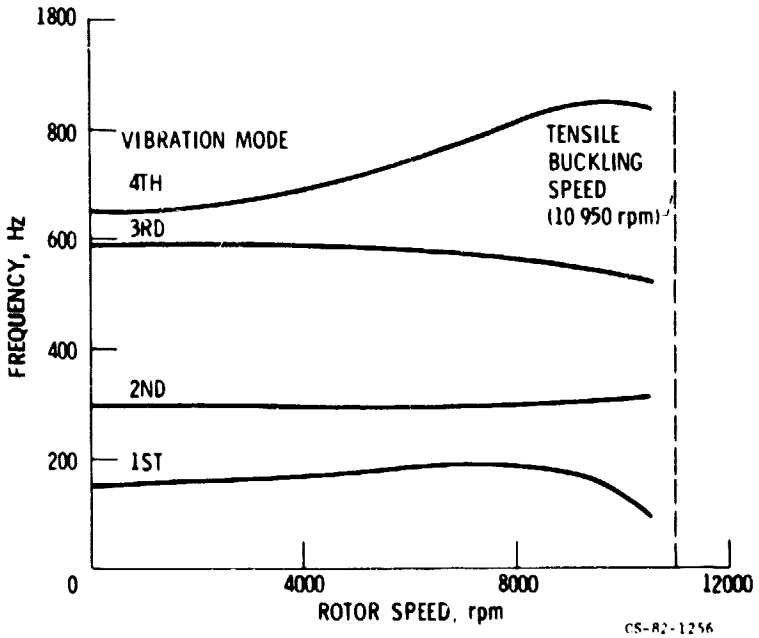


Figure 9. - Campbell diagram - 60° swept composite turboprop.

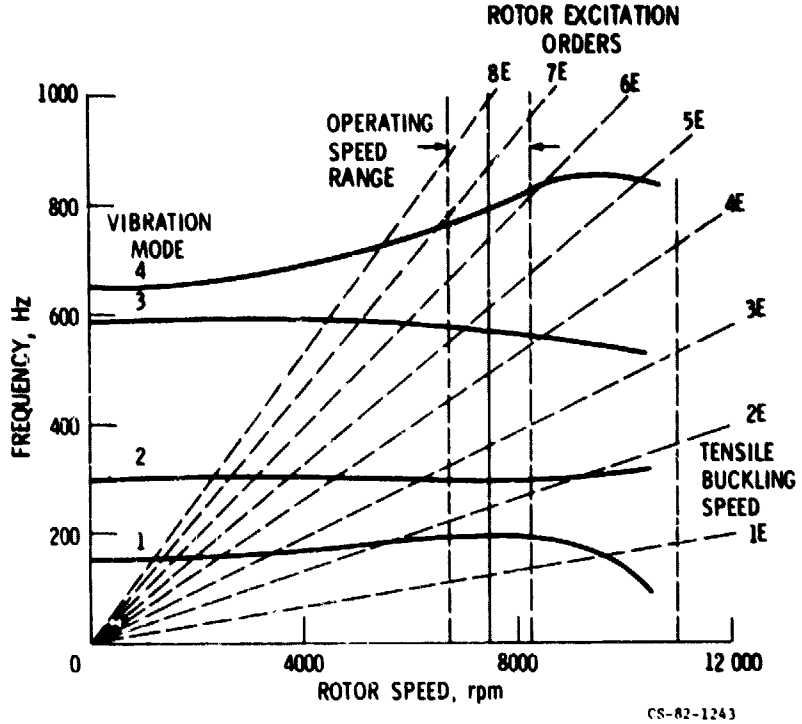


Figure 10. - Campbell diagram with rotor excitations.

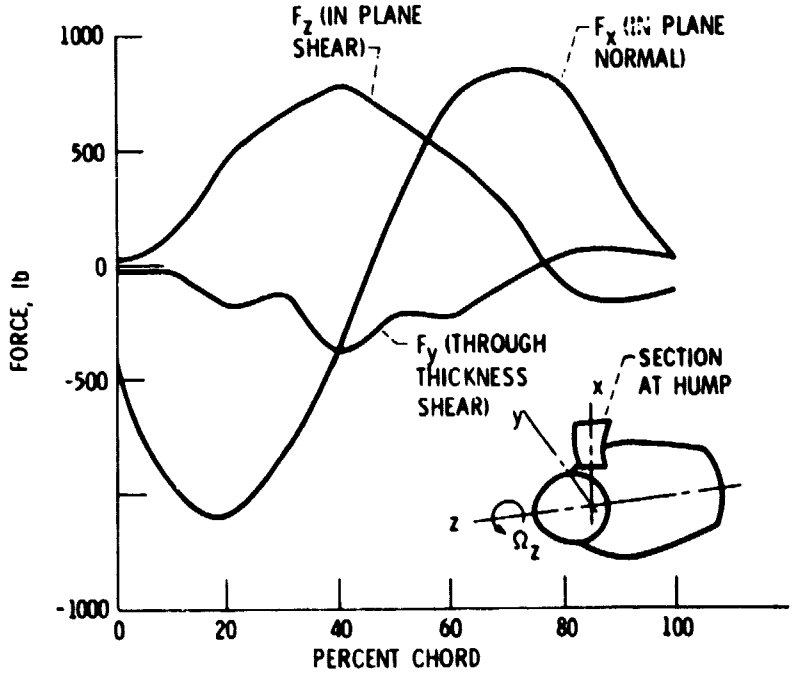


Figure 11. - Forces at the hump in a titanium $60^0$ swept turboprops at 6000 rpm.

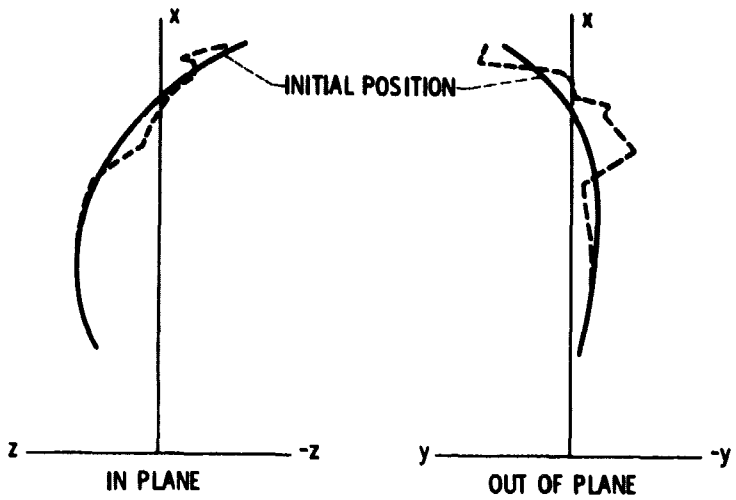


Figure 12. - Second tensile buckling modes of 60° swept composite turboprop.

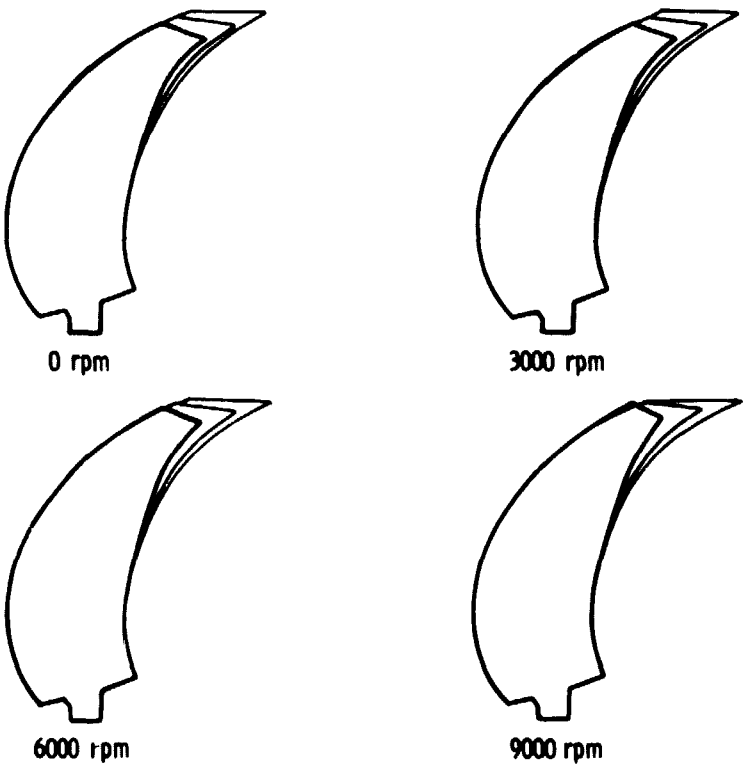


Figure 13. - Mode 1 vibrations of a 60° swept composite turboprop at various rotor speeds.

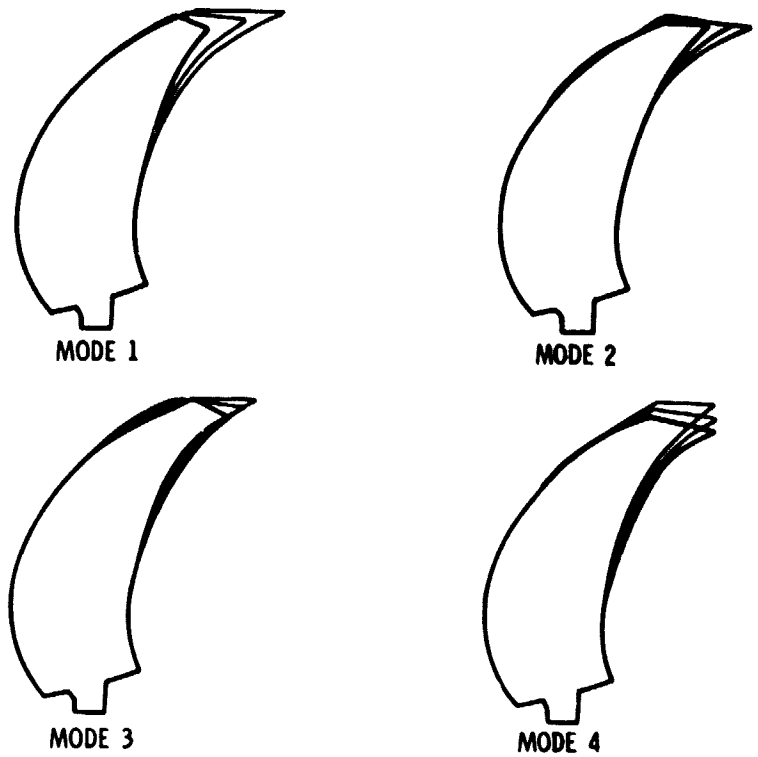


Figure 14. - Vibration modes of a $60^0$ swept composite turboprop at 7500 rpm rotor speed.

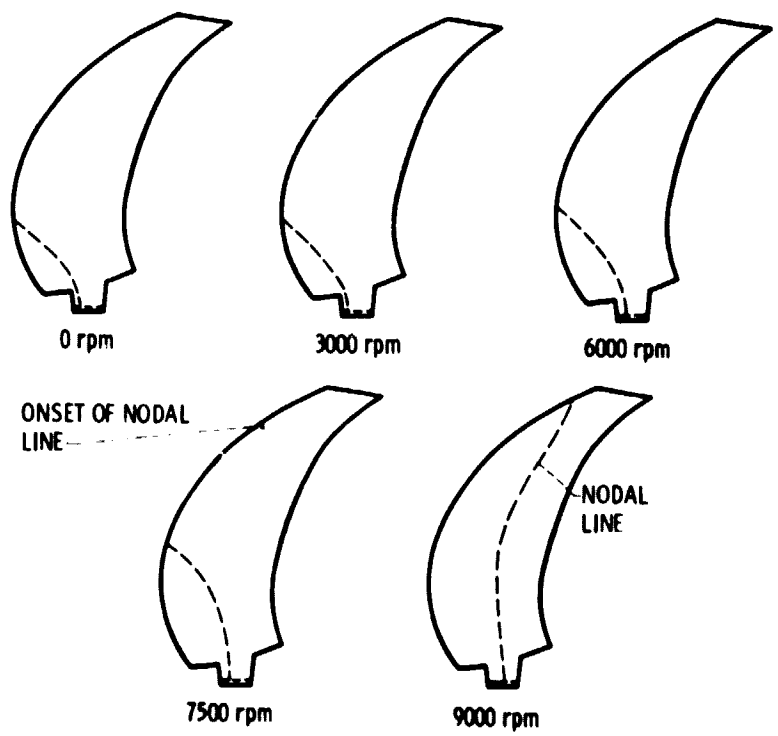


Figure 15. - Effects of rotor speed on the vibration mode 1 Nodal lines, $60^0$ swept composite turboprop.

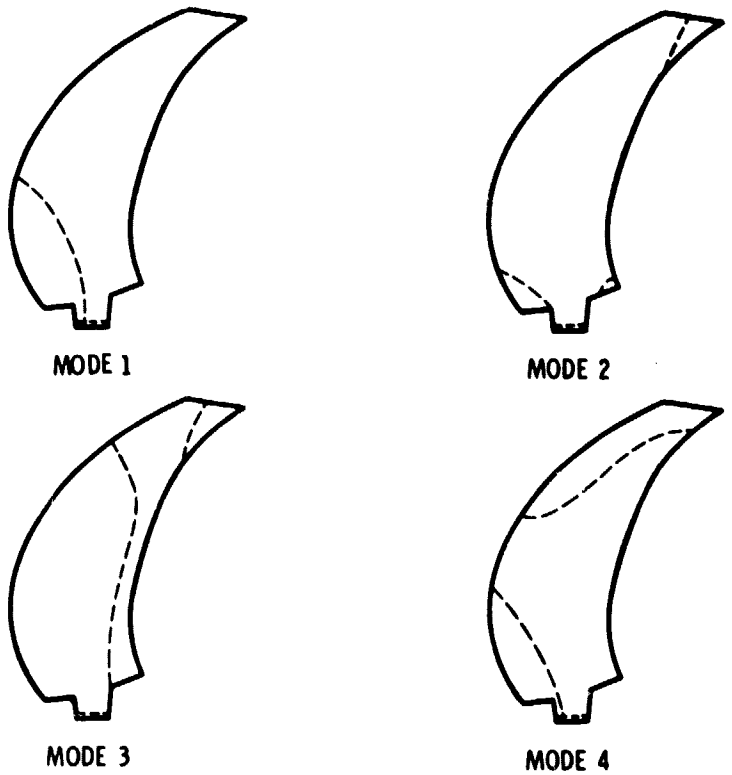


Figure 16. - Nodal lines of vibration modes, $60^{0}$ swept composite turboprop at 7500 rpm rotor speed.